energies

MDPI

Article

A Comprehensive Evaluation Method and Strengthening Measures for AC/DC Hybrid Power Grids

Junli Zhang, Guoteng Wang, Zheng Xu and Zheren Zhang *

College of Electrical Engineering, Zhejiang University, Hangzhou 310027, China; 11910064@zju.edu.cn (J.Z.); wgt339@zju.edu.cn (G.W.); xuzheng007@zju.edu.cn (Z.X.)
* Correspondence: zhangzheren@zju.edu.cn; Tel.: +86-18867104605

Abstract: Due to the complex operation characteristics of AC/DC hybrid power grids, it is a great challenge to comprehensively evaluate their stability and formulate appropriate strengthening schemes for them. To address this challenge, the following studies are carried out in this paper. First, an evaluation system including six indicators is established for AC/DC hybrid power grids. Next, aiming at the problems that may be revealed by the comprehensive evaluation, strengthening measures that can be utilized are introduced. Then, a comprehensive evaluation method for AC/DC hybrid power grids and their potential strengthening schemes is proposed. This method can deal with three issues, including normalization of the indicators, weighting of the indicators, and the trade-off of technology and cost. Finally, in the case study of the Qujing Power Grid, the main problems faced by regional power grids are pointed out, and four feasible strengthening schemes are formulated and evaluated.

Keywords: AC/DC hybrid power grid; evaluation indicator; strengthening measure; weighting method; trade-off of technology and cost

Citation: Zhang, J.; Wang, G.; Xu, Z.; Zhang, Z. A Comprehensive Evaluation Method and Strengthening Measures for AC/DC Hybrid Power Grids. *Energies* **2022**, *15*, 4432. https://doi.org/10.3390/en15124432

Academic Editor: Ahmed F. Zobaa

Received: 28 May 2022
Accepted: 16 June 2022
Published: 17 June 2022

1. Introduction

With the progress of transmission technologies, the State Grid of China has been a large-scale AC/DC hybrid power grid [1,2]. In recent years, multiple types of flexible transmission system equipment have been put into operation in the State Grid of China, such as the unified power flow controller (UPFC) and the high-voltage direct current (HVDC) system based on a voltage source converter (VSC) [3,4]. With the operation of various power electronic devices, the operation characteristics of this AC/DC hybrid power grid are becoming more and more complex.

A large-scale AC/DC hybrid power grid usually has the following characteristics: a high proportion of DC power to total load, large installed capacity of generators, and deficiency of control means [5]. These characteristics make a large-scale AC/DC hybrid power grid face some safety and stability problems [6,7]. In order to deal with these problems, a lot of technologies and devices can be used singly or in combination to form stability strengthening schemes. Considering the diversity of new technologies and the complexity of system operation characteristics, it is necessary to study the comprehensive stability strengthening schemes for AC/DC hybrid power grids, to help operators improve the power system stability on the premise of affordable economic investment.

At present, scholars have carried out a lot of research on AC/DC hybrid power grids, which mainly involves operation characteristics, simulation methods, control strategies, and stability evaluation methods. For example, the interaction between multiple VSC-HVDC systems and the receiving AC system under AC faults is studied in [8]. Ref. [9] presents an electromechanical–electromagnetic transient simulation system, in which the large AC/DC power grid is divided into small sub-networks. In [10], a control scheme of LCC-VSCs interlinking converters is introduced, which can help the AC/DC network operate stably under various conditions. Ref. [11] proposes an adaptive security risk assessment system for an electric power system, which is based on electricity regulation.

As for the evaluation methods and strengthening schemes for large-scale power grids, the existing research mainly focuses on certain equipment or one kind of stability problems. For example, some scholars proposed a method to calculate the AC short-circuit current near the converter station, considering the dynamic characteristics of the converter station [12]. In [13], the local load margin and some other indicators are applied to analyze the static voltage stability of power grids. Ref. [14] introduces a new indicator, the hybrid multi-infeed effective short-circuit ratio (HMESCR), to evaluate the power stability of hybrid multi-infeed HVDC systems. In [15], an analytical method based on multi-point linearization is applied to improve the accuracy of rotor angle stability analysis considering the influence of multi-terminal direct current (MTDC) systems. Ref. [16] studies the rotor angle stability indicator from the perspective of time-domain simulation. Ref. [17] discusses the rate of change of frequency (RoCoF) and its temporal and spatial aggregation. In [18], a method for evaluating the inertia demand is presented, considering the constraints of RoCoF and the frequency nadir. In [19], a method for evaluating the risk of commutation failure of the DC system after AC faults at the receiving end is proposed. However, an evaluation method considering only one single problem cannot measure a complex hybrid power grid in an all-around way. In addition, the existing research rarely takes the trade-off of technology and cost into account. Thus, how to comprehensively evaluate AC/DC hybrid power grids and their potential strengthening schemes integrating multi-dimensional technical evaluation and cost analysis needs to be further studied.

Obviously, the comprehensive evaluation of power systems can be regarded as a multi-criteria decision-making (MCDM) problem. In this regard, the research results obtained by mathematicians are worthy of reference. For example, the analytic hierarchy process (AHP) has been widely used to calculate subjective weights in MCDM problems since its birth [20–22]. The best worst method (BWM) is another commonly used subjective weight calculation method, which requires less data and can produce reliable results [23,24]. In terms of objective weight calculation, the entropy weight method (EWM) [25,26], the technique for order preference by similarity to ideal solution (TOPSIS) [27], and the critic method [28] are some of the recognized methods. Actually, the work of this paper is based on BWM and EWM.

The contributions of this paper are summarized as follows:

- An evaluation system including six indicators is established for AC/DC hybrid power grids, which covers various safety and stability issues.
- For various safety and stability issues, measures that can be utilized to solve them are introduced.
- A method for comprehensive evaluation of AC/DC hybrid power grids is proposed. Considering multiple dimensions to evaluate the safety and stability of the power system, this method can give technical scores for different schemes, and present curves reflecting the trade-off of the technical scores and the costs.

The remainder of this paper is organized as follows: Section 2 introduces six evaluation indicators, which are the basis of the technical analysis of AC/DC hybrid power grids. Section 3 summarizes some typical countermeasures for the problems faced by AC/DC hybrid power grids. Section 4 introduces, in detail, the comprehensive evaluation method. Then, the case study of the Qujing Power Grid is implemented in Section 5. Finally, Section 6 concludes this paper.

2. Evaluation System and Indicators

The evaluation system proposed in this paper covers the evaluation of short-circuit current, voltage stability, power angle stability, frequency stability, thermal stability, and DC fault. Indicators used in the system are described below.

2.1. Short-Circuit Current Margin

Statistics show that the influence of the three-phase metallic short-circuit fault is the most serious. Thus, the short-circuit current margin, K_{sci}, at bus i can be defined as follows:

$$K_{\mathrm{sc}i} = \frac{I_{\mathrm{bmax}i} - I_{\mathrm{sc}i}}{I_{\mathrm{bmax}i}} \times 100\% \tag{1}$$

Here, $I_{\mathrm{bmax}i}$ is the maximum allowable short-circuit current at bus i, which is usually the upper limit of the breaking capacity of the circuit breaker; $I_{\mathrm{sc}i}$ is the three-phase metallic short-circuit current at bus i. Obviously, the short-circuit current margin calculated according to (1) is a restrictive indicator. To ensure the safety of the power system, the short-circuit current margin of any bus should be positive. If $K_{\mathrm{sc}i} < 0$, it means that the short-circuit current at bus i exceeds the limit and the system has safety problems.

2.2. Local Load Margin

When analyzing the voltage stability of large-scale hybrid power grids, we usually focus on the impact of the load growth on bus voltage. Taking the power system shown in Figure 1a as an example. When analyzing the local static voltage stability at bus i, the original system can be simplified to an equivalent system using Thevenin's theorem, with the power flow at bus i remaining constant, as shown in Figure 1b.

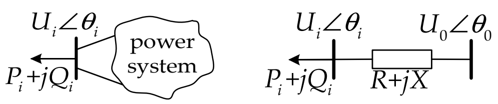

Figure 1. Partial schematic diagram of a power system. (**a**) The original system. (**b**) The equivalent system.

Then, some assumptions are made:

- The system is large enough so that the equivalent voltage, U_0, keeps unchanged during the load growth at bus i.
- The power factor angle at bus i, φ_i, keeps unchanged.
- The load at any other bus keeps unchanged, too.

Thus, the local load margin, $P_{\mathrm{Lmg}i}$, can be defined as (2):

$$P_{\mathrm{Lmg}i} = \frac{P_{i\,\mathrm{max}} - P_i}{P_{i\,\mathrm{max}}} \times 100\% \tag{2}$$

Here, P_i is the active power of the load at bus i, and $P_{i\mathrm{max}}$ is the critical power value, at bus i, that make system unstable. Apparently, the local load margin, $P_{\mathrm{Lmg}i}$, calculated by (2), is a restrictive indicator. To ensure the safety and stability of the power system, the local load margin should be greater than 0. The larger the margin is, the better the static voltage stability of the corresponding bus is. Based on engineering experience, the local load margin of every bus should be greater than 8% in normal conditions.

Based on the assumptions, we have [29]:

$$U_0 = \sqrt{\left(U_i + \frac{P_i R + Q_i X}{U_i}\right)^2 + \left(\frac{P_i X - Q_i R}{U_i}\right)^2} \tag{3}$$

$$P_i \sin\varphi_i = Q_i \cos\varphi_i \tag{4}$$

Accordingly, the expression of P-U curve at bus i, $U_i = f(P_i)$, can be obtained:

$$\begin{cases} P_i = \frac{U_i^2 \cos\varphi_i}{R^2+X^2}\left(\sqrt{A^2 + \frac{U_0{}^2R^2+U_0{}^2X^2}{U_i{}^2}} - R^2 - X^2 - A\right) \\ A = R\cos\varphi_i + X\sin\varphi_i \end{cases} \tag{5}$$

Here, A is an intermediate variable for ease of representation.

As shown in Figure 2, the voltage and power at the rightmost end of the P-U curve at bus i are named as $U_{\mathrm{lmt1},i}$ and $P_{\mathrm{lmt1},i}$.

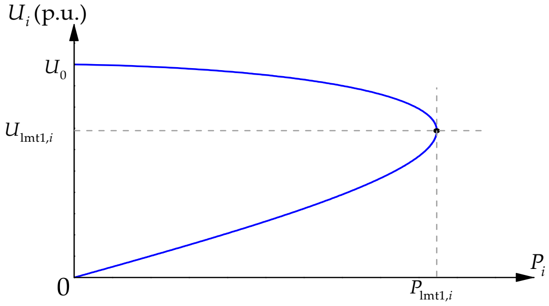

Figure 2. The P-U curve at bus i (parameters take typical values).

Apparently, the active load, P_i, is not allowed to exceed $P_{\mathrm{lmt1},i}$, otherwise voltage collapse will occur in the system. According to (5), the value of $U_{\mathrm{lmt1},i}$ can be obtained:

$$U_{\mathrm{lmt1},i} = \frac{U_0 \cdot \sqrt{2(Z^2 - AZ)}}{2\,|X\cos\varphi_i - R\sin\varphi_i|} \tag{6}$$

In addition, for the safety of the equipment, the operating voltage, U_i, must be within a reasonable range. Actually, considering the trend of typical P-U curves, the lower limit of U_i should be mainly concerned, which can be expressed as $U_{\mathrm{lmt2},i}$. In real power systems, $U_{\mathrm{lmt2},i}$ is usually taken as 0.9. Then, the minimum allowed value of U_i can be obtained as:

$$U_{i\,\mathrm{min}} = \max\{U_{\mathrm{lmt1},i}, U_{\mathrm{lmt2},i}\} \tag{7}$$

When $U_i = U_{i\mathrm{min}}$, P_i in (5) will be the critical power value.

2.3. Critical Clear Time of Fault

The critical clear time of a fault, t_{cr}, can be used to evaluate the large disturbance rotor angle stability of the system. For any fault in the system, if its duration exceeds its t_{cr}, at least one generator will lose synchronization with the system, which means that rotor angle instability will occur. Considering the occurrence probability and the harm, the fault category analyzed in this paper is the three-phase metallic short-circuit fault at the end of a transmission line.

Take the two-area interconnected power system shown in Figure 3 as an example. In this system, two lines constitute a transmission channel between bus i and bus j, and P_{T} is the active power transmitted through the channel. The rest of the power system is simplified, which is represented by two regional equivalent generators (G1/G2) and two equivalent transformers (T1/T2).

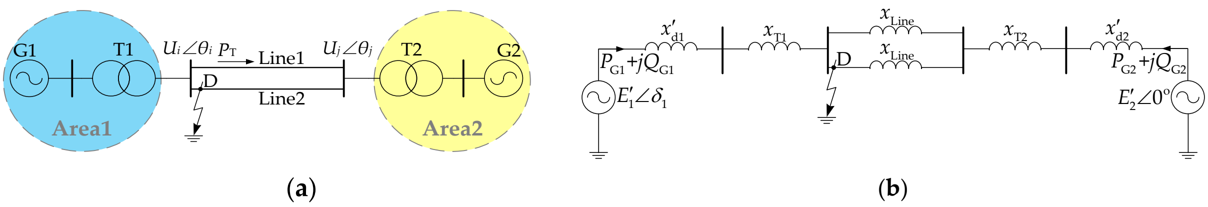

Figure 3. A typical two-area interconnected power system. (**a**) The wiring diagram. (**b**) The circuit diagram.

For the convenience of calculation, several assumptions are made:

- For generators, the second-order model is used [29]. In this model, the amplitude of the transient potential, E', remains unchanged for a short time after the fault.

- The inertia time constants of the generators, T_{JG1}/T_{JG2}, are calculated using the base power of the system, while T_{JG2} is larger than T_{JG1}.
- The rotor angle of G2 is set as the reference angle.
- For each line, the reactance is x_{Line}, and its resistance is negligible compared with x_{Line}.
- For each transformer, the resistance is negligible.

As shown in Figure 3, a three-phase metallic short-circuit fault occurs on Line2. According to the assumptions, it is easy to find that this fault has a greater impact on G1. In this case, the critical clear time of the fault can be estimated using the following formula (for details, see Appendix A):

$$\begin{cases} t_{cr} = \sqrt{\dfrac{2T_{JG1} \cdot \left\{\cos^{-1}[\cos\delta_{1h} + (\delta_{1h} - \delta_{1\_0})\sin\delta_{1h}] - \delta_{1\_0}\right\}}{\omega_N P_{G1\_0}{}^*}} \\ \delta_{1h} = \pi - \sin^{-1}\left(\dfrac{x'_{d1}{}^* + x'_{d2}{}^* + x_{T1}{}^* + x_{T2}{}^* + x_{Line}{}^*}{x'_{d1}{}^* + x'_{d2}{}^* + x_{T1}{}^* + x_{T2}{}^* + 0.5x_{Line}{}^*}\sin\delta_{1\_0}\right) \end{cases} \tag{8}$$

Here, the variables with subscript 0 are values before the fault; the variables with superscript * are per-unit values; P_{G1} is the active power output by G1; x with different subscripts is the reactances in the system, as shown in Figure 3; ω_N is the rated electric angular velocity of the rotor; δ_{1h} is an intermediate variable for ease of derivation.

If the two areas in that system are also connected through a VSC-DC system, as shown in Figure 4, the result will be different. On the one hand, P_T can be changed by adjusting the power transmitted by the DC system, so as to enlarge t_{cr}. On the other hand, the active power absorbed by VSC1 and VSC2 from the AC system can also be controlled after the fault, so as to change the "acceleration area" and "deceleration area" in the analysis of equal area criterion. In this way, the critical clear time of the fault can be estimated using the following formula (for details, see Appendix A):

$$\begin{cases} t_{cr} = \sqrt{\dfrac{2T_{JG1} \cdot \left\{\cos^{-1}[\cos\delta_{1h}{}' + (\delta_{1h}{}' - \delta_{1\_0})\sin\delta_{1h}{}'] - \delta_{1\_0}\right\}}{\omega_N (P_{G1\_0}{}^* - \Delta P_{VSC1}{}^*)}} \\ \delta_{1h}{}' = \pi - \sin^{-1}\left[\dfrac{(P_{G1\_0}{}^* - \Delta P_{VSC1}{}^*)x_{\Sigma 1}{}^*}{E_1'{}^* E_2'{}^*}\right] \\ x_{\Sigma 1}{}^* = x'_{d1}{}^* + x'_{d2}{}^* + x_{T1}{}^* + x_{T2}{}^* + x_{Line}{}^* \end{cases} \tag{9}$$

Here, the variables with subscript 0 are values before the fault; the variables with superscript * are per-unit values; $\Delta P_{VSC1}{}^*$ is the increase of the power absorbed by VSC1 from the AC system; $\delta_{1h}{}'$ and $x_{\Sigma 1}{}^*$ are intermediate variables.

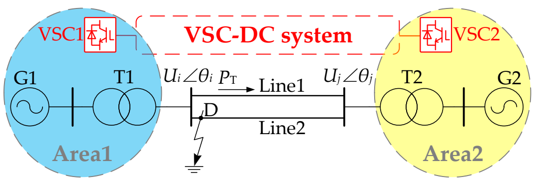

Figure 4. A typical two-area power system, including a VSC-DC system.

For faults in other scenarios, t_{cr} can be calculated similarly. Of course, in a complex power system, it is more convenient to get the value of t_{cr} by time simulation.

Apparently, the critical clear time of a fault, t_{cr}, is a restrictive indicator. To ensure the safety and stability of the power system, t_{cr} should be strictly greater than the expected clear time for any fault, that is:

$$t_{cr} > t_f \tag{10}$$

Here, t_f is the expected clear time of the fault, that is, the sum of delay time and action time of the main protection mechanism. For three-phase metallic short-circuit faults, t_f can be estimated as 0.1 s.

Since t_{cr} does not have a reasonable upper limit, it can also be expressed in the form of margin, K_{time}, as shown below:

$$K_{time} = \frac{t_{cr} - t_f}{t_{cr}} \times 100\% \tag{11}$$

Apparently, K_{time} is a restrictive indicator, which should be strictly greater than zero.

2.4. Thermal Stability Margin

To limit the heating effect, there is a maximum allowable value of the apparent power that can be transmitted by a transmission line or a transformer. For line i or transformer i, this limit can be expressed as $S_{i\max}$. Then, the thermal stability margin of line i or transformer i can be defined as ξ_i [29]:

$$\xi_i = \frac{S_{i\max} - S_i}{S_{i\max}} \times 100\% \tag{12}$$

Here, S_i is the apparent power actually transmitted by line i or transformer i.

When the system operates in different conditions, S_i will be different, resulting in a different value of ξ_i. Therefore, in order to avoid confusion, a unified method for calculating ξ_i is given in this paper.

- Calculate S_i successively in normal conditions and all the "single maintenance conditions". Here, a "single maintenance condition" is a condition that there is only one transmission channel or one transformer in the system that is out of operation due to maintenance.
- Substitute the maximum S_i obtained in the previous step into (12) to calculate ξ_i.

If there are devices that can control the power flow in the system, the influence of them needs to be considered in the calculation of S_i. Of course, when calculating the apparent power of different transformers or lines, it should be ensured that the influence of these power flow control devices stays consistent in the same operating condition.

Apparently, the thermal stability margin, ξ_i, calculated by (12), is a restrictive indicator. For the safety and stability of the power system, its value should be greater than a positive value given according to actual needs (usually 10%). The larger the value is, the better the thermal stability of the transmission channel or substation is.

2.5. Rate of Change of Frequency

To explain the definition of the rate of change of frequency, we can take a single generator with load as an example. For the generator, the rotor motion equation is [29]:

$$T_J \frac{d\omega^*}{dt} = {P_m}^* - {P_e}^* \tag{13}$$

Here, ${P_m}^*$ is the per unit value of the mechanical power; ${P_e}^*$ is the per unit value of the electromagnetic power; T_J is the inertia time constant calculated using the base power of the system; ω^* is the per-unit value of the electric angular velocity.

In a steady state, ${P_m}^*$ is equal to ${P_e}^*$. Thus, assuming that ${P_m}^*$ keeps unchanged when a disturbance, $\Delta{P_e}^*$, occurs, we have:

$$\frac{d\omega^*}{dt} = \frac{{P_m}^* - ({P_e}^* + \Delta{P_e}^*)}{T_J} = -\frac{\Delta{P_e}^*}{T_J} \tag{14}$$

So, we can use the rate of change of frequency to evaluate the frequency stability of the system, which is defined as μ [17]:

$$\mu = \frac{df}{dt} = f_N \cdot \frac{d\omega^*}{dt} = -\frac{f_N \Delta{P_{max}}^*}{T_J} \tag{15}$$

Here, $\Delta P_{\text{max}}{}^{*}$ is the maximum change of power that may occur when a single power supply or load is cut off after the fault, which is positive when a load is cut off and negative when a power supply is cut off. f and f_{N} are the actual frequency and the rated frequency of the system, respectively. T_{J} is calculated after the cutting-off. In this way, μ can reflect the instantaneous rate of change of frequency at the moment of the cutting-off.

Considering the ability of some equipment to quickly control the active power, Equation (15) can be modified as:

$$\mu = \frac{f_{\text{N}}(\Delta P_{\text{max}}{}^{*} - \Delta P_{\text{ctrl}}{}^{*})}{T_{\text{J}}} \tag{16}$$

Here, $\Delta P_{\text{ctrl}}{}^{*}$ is the maximum change of active power that can be obtained immediately by the control of existing equipment, on the premise of safety and stability. More clearly, if $\Delta P_{\text{ctrl}}{}^{*}$ is positive, it means that the control leads to the increase of power supplies or the decrease of load power. The rate of change of frequency, μ, is a restrictive indicator. For the safety and stability of the power system, it should be always within the specified range (usually the upper and lower limits are ± 0.5 Hz/s). The closer it is to zero, the better the frequency stability of the system is.

2.6. Proportion of Buses Related to Commutation Failure

For an HVDC system based on a line commutated converter (LCC), the commutation failure is the most common fault of the inverter, which has a serious impact on the safety and stability of the receiving system.

If the three-phase metallic short-circuit fault of AC bus i will cause the commutation failure of LCC-HVDC system j, then bus i can be named as a bus related to the commutation failure of the LCC-HVDC system j. Thus, for LCC-HVDC system j, the proportion of buses related to commutation failure of it, $K_{\text{fail}j}$, can be defined as:

$$K_{\text{fail}j} = \frac{n_{\text{fail}j}}{N_{\text{tot}}} \times 100\% \tag{17}$$

Here, $n_{\text{fail}j}$ is the number of buses related to commutation failure of DC system j, and N_{tot} is the total number of AC buses in the power grid.

Strictly speaking, in order to obtain the exact results of $n_{\text{fail}j}$ and $K_{\text{fail}j}$, it is necessary to perform fault analysis for all AC buses by time-domain simulation. However, when the accuracy requirement is not very high, a rough judgment can also be made according to the following formula [14]:

$$MIIF_{j,i} = \frac{\Delta U_j}{\Delta U_i} > 0.15 \tag{18}$$

Here, $MIIF_{j,i}$ is the multi-infeed interaction factor (MIIF) from bus i to the inverter station of DC system j; ΔU_i is the voltage disturbance at bus i; and ΔU_j is the corresponding AC bus voltage variation at the inverter station of DC system j.

If (18) is true, bus i can be roughly regarded as a bus related to commutation failure of DC system j. This is because the commutation failure usually occurs when the AC voltage at the inverter station suddenly drops below 0.85 p.u., and MIIF can be used to estimate the voltage variation at a bus due to the voltage disturbance at another bus.

The proportion of buses related to commutation failure of LCC-HVDC system j, $K_{\text{fail}j}$, is a comparative indicator; the larger it is, the higher the probability of commutation failure of LCC-HVDC system j is.

3. Strengthening Measures for AC/DC Power Grids

3.1. Measures for a Single Problem

3.1.1. Measures to Enlarge the Short-Circuit Current Margin

If the bus with an insufficient short-circuit current margin exists alone, priority shall be given to whether it can be improved by replacing the circuit breaker. If the short-circuit current margins of the buses in a certain area are generally small, they can be considered to reduce generators, appropriately increase the electrical distance from that area to other areas, or even upgrade the voltage level.

3.1.2. Measures to Improve the Static Voltage Stability

If the local load margin of an area or a bus is very small, it indicates that the static voltage stability there is insufficient. Then, operators can increase generators, decrease the electrical distance from that area to other areas, or build dynamic reactive power compensation devices such as a static synchronous compensator (STATCOM).

3.1.3. Measures to Reduce the Risk of Transient Instability

If the minimum critical clear time of fault in the system is very small, it indicates that the risk of transient instability is relatively large. At this time, feasible measures include building new AC or DC transmission lines at corresponding transmission sections, and building some power flow control devices, such as a UPFC, to adjust the power flow.

3.1.4. Measures to Improve the Thermal Stability

There are two main reasons for insufficient thermal stability margin. One is the insufficient capacity, for which a feasible response measure is to build some new transmission lines or transformers. The other is the uneven distribution of power flow, for which a feasible countermeasure is to build new power flow control devices to adjust the operating condition of the system.

3.1.5. Measures to Improve the Frequency Stability

If the emergency removal of a load makes the system's frequency rise too fast, the load should be split. Similarly, if the removal of a power supply makes the system's frequency drop too fast, it could be considered to split it or reduce its capacity. In addition, building flexible AC transmission systems (FACTS) and building VSC-DC systems are also feasible measures, because these devices can quickly adjust the active power.

3.1.6. Countermeasures to Commutation Failure

If the probability of commutation failure of a single DC system is high, increasing the electrical distance from its converter bus to other AC buses and building reactive power compensation devices are feasible measures. If multiple DC systems in a certain area are likely to have commutation failure at the same time, transforming conventional DC systems into DC systems based on VSC is a good countermeasure.

3.2. Measures for Comprehensive Problems

As analyzed above, countermeasures to different problems may be conflicting, which means that comprehensive analysis is sometimes required. For example, two common comprehensive problems in large-scale AC/DC hybrid grids are introduced below:

3.2.1. Coordination of Voltage Stability and Short-Circuit Current Margin

If the short-circuit current margin is large enough but the static voltage stability is poor, priority can be given to increasing generators or building new AC transmission lines. If the static voltage stability is good enough but the short-circuit current margin is small, priority can be given to reducing generators or disconnecting some AC transmission lines.

However, sometimes the static voltage stability is poor while the short-circuit current margin is small. At this time, the static voltage stability can only be improved by building reactive power compensation devices, such as STATCOM, that hardly provide a short-circuit current. The short-circuit current margin can only be improved by replacing the circuit breaker or upgrading the voltage level.

3.2.2. Coordination of Static Voltage Stability and the Problem of Commutation Failure

If the impact of the commutation failure is not serious, building new AC transmission lines is feasible to improve the static voltage stability. If the static voltage stability is good enough, it is feasible to disconnect some AC transmission lines to reduce the probability of commutation failure.

However, sometimes these two problems both need to be dealt with. At this time, it is feasible to build some reactive power compensation devices, as poor static voltage stability and high probability of commutation failure are both the manifestations of insufficient reactive power to some extent. In addition, it can be considered to transform some conventional DC systems into VSC-based DC systems, or build a VSC-based MTDC system. These measures can solve the problem of commutation failure from the root and improve the static voltage stability.

4. Comprehensive Evaluation Method

The evaluation of AC/DC hybrid power grids and the strengthening schemes of them is a comprehensive problem, which is divided into three issues in this paper.

4.1. Normalization of the Indicators

Since different indicators vary greatly in units and values, their values should be normalized. The purpose of this task can be set as: the normalized value of each indicator is always between 0 and 1, with 0 representing the worst value that can be tolerated and 1 representing the best value that may appear.

For some of the indicators, a larger original result means that the security or stability is better. The normalization equation of these indicators can be given as:

$$r_{ij} = \frac{R_{ij} - R_{j\min}}{R_{j\max} - R_{j\min}} \tag{19}$$

On the contrary, for the other indicators, smaller values are better. For them, the normalization equation can be given as:

$$r_{ij} = \frac{R_{j\max} - R_{ij}}{R_{j\max} - R_{j\min}} \tag{20}$$

In (19) and (20): $R_{j\max}$ is the maximum allowable value of the j-th indicator; $R_{j\min}$ is the minimum allowable value of the j-th indicator; R_{ij} is the original result of the j-th indicator under the i-th situation; r_{ij} is the normalized value of R_{ij}. The suggested reference values, $R_{j\max}$ and $R_{j\min}$, of the six indicators proposed in this paper, are shown in Table 1.

Table 1. Reference values for the normalization.

Number	Indicator	$R_{j\max}$	$R_{j\min}$	Suitable Formula
1	$K_{\mathrm{sc}i}$	100%	0	(19)
2	$P_{\mathrm{Lmg}i}$	100%	8%	(19)
3	K_{time}	100%	0	(19)
4	ξ_i	100%	10%	(19)
5	μ	0.5 Hz/s	0	(20)
6	$K_{\mathrm{fail}j}$	100%	0	(20)

In Table 1, as it is difficult to give a reasonable upper limit of t_{cr}, K_{time} is used instead of it. The rate of change of frequency, μ, is used in the form of an absolute value.

4.2. Weighting of the Indicators

When comprehensively evaluating AC/DC hybrid power grids, it is necessary to conduct a technical analysis by utilizing the six indicators introduced in this paper. Apparently, it is a MCDM problem, in which the weighting of the indicators is very important. Therefore, a weighting method is put forward in this paper. Specifically, BWM and EWM are used to calculate the subjective weights and the objective weights, and the minimum discriminant information principle [30] is used to obtain the combined weights.

4.2.1. Subjective Weights

Specific steps of using BWM to calculate subjective weights are as follows [23]:

(a) Determine a set of decision evaluation indicators, such as $[R_1, R_2, \ldots, R_\mathrm{n}]$.
(b) Choose the best (most important) indicator and the worst indicator.
(c) Determine the priority of the best indicator over other indicators, using an integer between 1 and 9 inclusive. The resulting best-to-others vector would be:

$$\boldsymbol{P}_{\mathbf{B}} = (p_{\mathrm{B}1},\ p_{\mathrm{B}2},\ \ldots\ ,\ p_{\mathrm{B}n}) \tag{21}$$

here, $p_{\mathrm{B}j}$ is the priority of the best indicator over the j-th indicator. Particularly, $p_{\mathrm{BB}} = 1$.

(d) Determine the priority of other indicators over the worst indicator, using an integer between 1 and 9 inclusive. The resulting others-to-worst vector would be:

$$\boldsymbol{P}_{\mathbf{W}} = (p_{1\mathrm{W}},\ p_{2\mathrm{W}},\ \ldots\ ,\ p_{n\mathrm{W}}) \tag{22}$$

here, $p_{j\mathrm{W}}$ is the priority of the j-th indicator over the worst indicator. Particularly, $p_{\mathrm{WW}} = 1$.

(e) Considering the non-negativity and the sum condition of the subjective weights, we should solve such an optimization problem to calculate the subjective weights:

$$\begin{cases} \min \max\limits_{j} \left\{ \left| \frac{w_{\mathrm{B}}\prime}{w_j\prime} - p_{\mathrm{B}j} \right|,\ \left| \frac{w_j\prime}{w_{\mathrm{W}}\prime} - p_{j\mathrm{W}} \right| \right\} \\ \text{s. t.} \sum_{j=1}^{n} w_j\prime = 1 \\ \quad w_j\prime \geq 0,\ \ j = 1,\ 2,\ \ldots\ ,\ n \end{cases} \tag{23}$$

here, $w_j{}'$ is the subjective weight of the j-th indicator; $w_{\mathrm{B}}{}'$ is the subjective weight of the best indicator; $w_{\mathrm{W}}{}'$ is the subjective weight of the worst indicator.

4.2.2. Objective Weights

Specific steps of using EWM to calculate objective weights are as follows [25]:

(a) Select m situations from the current situation and the situations after the application of feasible strengthening schemes.
(b) For each selected situation, calculate the normalized values of all the n indicators. For each indicator, only one smallest normalized result should be retained.
(c) Calculate the entropy value of each indicator, Ej, as:

$$\begin{cases} E_j = -\frac{1}{\ln n} \sum_{i=1}^{m} q_{ij} \ln(q_{ij}) \\ q_{ij} = \frac{r_{ij}}{\sum_{i=1}^{m} r_{ij}} \end{cases} \tag{24}$$

here, q_{ij} is an intermediate variable for ease of representation. Then, the objective weight of the j-th indicator, $w_j{}''$, can be calculated as:

$$w_j{}'' = \frac{(1 - E_j)}{\sum\limits_{k=1}^{n} (1 - E_k)} \tag{25}$$

When the difference between some schemes only lies in the parameters of the equipment, only the one that brings the greatest change should participate in the calculation of objective weights. The reasons are: First, the influence of these schemes on the dispersion of indicator values is similar, so it is not necessary to include them all in the calculation; second, schemes that can lead to greater changes provide more useful information.

4.2.3. Combined Weights

To ensure that the combined weights are not biased to any one of the subjective and objective weights, an optimization model is established based on the minimum discriminant information principle to determine the combined weights [30]:

$$\begin{cases} \min \ \sum_{j=1}^{n} \left(w_j \ln \frac{w_j}{w_j{'}} + w_j \ln \frac{w_j}{w_j{''}} \right) \\ \text{s. t.} \ \sum_{j=1}^{n} w_j = 1, w_j \geq 0 \end{cases} \tag{26}$$

Here, w_j is the combined weight of the j-th indicator.

Solving (26), the expression of the final combined weights can be given as:

$$w_j = \frac{\sqrt{w_j{'} w_j{''}}}{\sum_{k=1}^{n} \sqrt{w_k{'} w_k{''}}} \tag{27}$$

4.3. Trade-Off of Technology and Cost

Finally, we can calculate the technical scores and the costs for strengthening schemes, and then draw the technology-cost curves reflecting the relationships between the technical scores and the costs. According to the curves, the trade-off of technology and cost can be executed in the planning.

4.3.1. Calculation of the Technical Score

The technical score of the i-th scheme, $s_{\mathrm{T}i}$, is calculated as:

$$s_{\mathrm{T}i} = \sum_{j=1}^{n} w_j r_{ij} \tag{28}$$

Apparently, the value range of $s_{\mathrm{T}i}$ is 0 to 1. If $s_{\mathrm{T}i} = 1$, it means that the safety or stability of the power system will achieve the optimal level in terms of each indicator with the i-th scheme applied. If $s_{\mathrm{T}i} = 0$, it indicates that the safety or stability of the power system will be at the worst level in terms of each indicator with the i-th scheme applied.

4.3.2. Calculation of the Total Costs

Several assumptions about the total cost of strengthening schemes are considered:

(a) Costs (F) consists of variable costs (F_1) and fixed costs (F_2). That is, for the i-th scheme, we have:

$$F(i) = F_1(i) + F_2(i) \tag{29}$$

(b) Here, F1 refers to the manufacturing and assembly costs of equipment, which could be assumed to be proportional to the total capacity of the equipment.

(c) Here, F2 refers to other costs, which are assumed to be fixed when the equipment capacity changes in this paper.

4.3.3. Drawing of the Technology-Cost Curve

For the i-th scheme, the values of $s_{\mathrm{T}i}$ and F_i can always be calculated corresponding to the total capacity of different equipment. Thus, a curve can be drawn to represent the change of F_i with respect to $s_{\mathrm{T}i}$, which is named as the technology-cost curve of the i-th scheme in this paper.

Limited by the equipment manufacturing level and the feasibility constraints, the curves of different schemes may be discontinuous or have a different abscissa range. For example, Section 5.4.1 shows the technology-cost curves of three different schemes.

By comparing the technology-cost curves, planners can easily judge the application values of strengthening schemes for an AC/DC hybrid power grid.

5. Case Study

To verify the comprehensive evaluation method proposed in this paper, a case study of the Qujing Power Grid, Yunnan Province, China, is implemented.

Yunnan Province is a province in Southwest China. Interconnected asynchronously with several other provincial power grids through HVDC systems, the Yunnan Power Grid is sending out a large amount of electricity power to other provinces. Meanwhile, due to the low level of local development, the internal transmission capacity of the Yunnan Power Grid is relatively weak. In this context, as one of the parts with the most concentrated load and export channels of the Yunnan Power Grid, the Qujing Power Grid may face some stability and security problems, which is worthy of analysis.

5.1. Current Situation of Qujing Power Grid

In flood season, part of the active power of Wudongde Hydropower Station needs to be fed into Longhai Substation and Baiyi Substation, as shown in Figure 5. However, the load and the export channels are mainly concentrated in Qujing and nearby areas. As a result, a large amount of active power is transmitted on the transmission section (indicated by the red dotted line in Figure 5), posing a threat to the power grid.

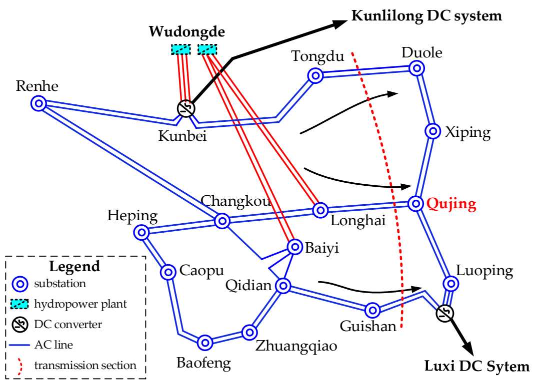

Figure 5. Partial structure of Yunnan 500 kV Power Grid.

As shown in Figure 6, there are electromagnetic ring networks in the Qujing Power Grid, composed of 500 kV lines, 220 kV lines, and several substations. Analysis shows that the electromagnetic ring networks are difficult to untie. However, if the situation remained, the Qujing Power Grid will have the problem of an insufficient thermal stability margin, which is common in regional power grids. The details of this problem are listed in Table 2.

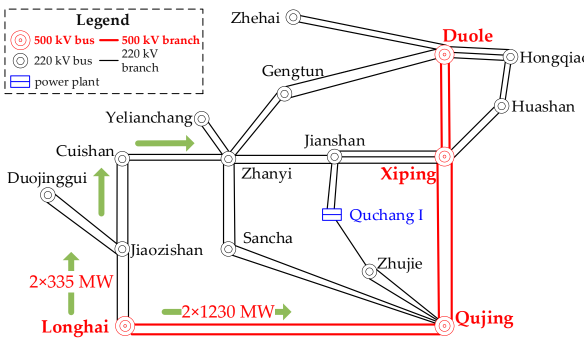

Figure 6. Structure of Qujing Power Grid.

Table 2. Single maintenance conditions in which the problem of insufficient thermal stability margin of lines will occur in Qujing Power Grid.

Maintenance Line	Line i with Insufficient Thermal Stability	S_i/MVA	$S_{i\max}$/MVA	ξ_i/%
both 500 kV lines from Longhai to Qujing	220 kV lines from Longhai to Jiaozishan	1149.5	1075.6	−6.87
	220 kV lines from Jiaozishan to Cuishan	1074.7	1075.6	0.08
	220 kV lines from Cuishan to Zhanyi	1010.8	1075.6	6.02
one 500 kV line from Longhai to Qujing	the other 500 kV line from Longhai to Qujing	2609.9	2728.0	4.33
one 220 kV line from Longhai to Jiaozishan	the other 220 kV line from Longhai to Jiaozishan	488.54	537.8	9.16

Other evaluation indicators are also applied, as shown in Tables 3–6, and it should be noted that the original result of K_{fail} is always zero since there is no inverter station in the Qujing Power Grid.

Table 3. The minimum short-circuit current margin in Qujing Power Grid.

Location (Bus i)	$I_{\mathrm{sc}i}$/kA	$I_{\mathrm{bmax}i}$/kA	$K_{\mathrm{sc}i}$/%
Longhai 500 kV Bus	37.85	63.00	39.92

Table 4. The minimum local load margin in Qujing Power Grid.

Location (Bus i)	$P_{i\max}$/MW	P_i/MW	$P_{\mathrm{Lmg}i}$/%
Tiangao 220 kV Bus	814.30	204.00	74.95%

Table 5. The minimum critical clear time of fault in Qujing Power Grid.

Location of the Fault	t_{cr}/s	t_{f}/s	K_{time}/%
near Longhai 500 kV Bus	0.282	0.1	64.54

Table 6. The maximum rate of change of frequency after a single piece of equipment is suddenly cut off in Qujing Power Grid.

Type of Equipment Cut Off	T_{J}/s	f_{N}/Hz	$\Delta P_{\max}{}^{*}$/p.u.	μ/Hz·s^{-1}
load (DC rectifier station)	8.7348	50	+0.031471	+0.18015
power supply	8.7314	50	−0.010816	−0.06194

To sum up, it is necessary to apply a strengthening scheme to solve the problem of an insufficient thermal stability margin in the Qujing Power Grid.

5.2. Feasible Strengthening Schemes

Based on the local conditions, four feasible strengthening schemes are formulated.

5.2.1. Scheme 1–Scheme 3: Build New AC Lines

Building 500 kV AC lines is a measure considered in this case. According to the current and planning situation of the Qujing Power Grid, the following three feasible strengthening schemes are put forward, of which the conductor model can be selected from those types shown in Table 7.

- *Scheme 1*: Build 500 kV double circuit lines from Longhai to Duole, of which the length is 99 km, as shown in Figure 7.
- *Scheme 2*: Build 500 kV double circuit lines from Longhai to Xiping, of which the length is 82 km, as shown in Figure 7.
- *Scheme 3*: Build 500 kV double circuit lines from Longhai to Guishan, of which the length is 79 km, as shown in Figure 7.

Table 7. Main parameters of optional conductors.

Number	Conductor Model	Sectional Area	Total Capacity
1	4 × JL/G1A-400/35	4 × 400 mm^2	2618.86 MVA
2	4 × JL/G1A-500/45	4 × 500 mm^2	3273.58 MVA
3	4 × JL/G1A-630/45	4 × 630 mm^2	4124.70 MVA

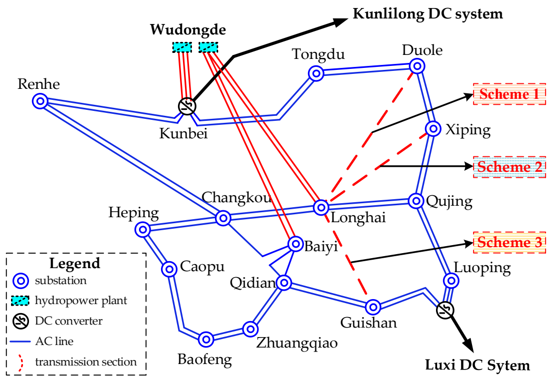

Figure 7. Sketch map of Scheme 1, Scheme 2, and Scheme 3.

5.2.2. Scheme 4: Build a UPFC

As shown in Figure 6, the lines that have problems of an insufficient thermal stability margin are connected in a series, while the problem of the 220 kV lines from Longhai to Jiaozishan is the most serious. Thus, we have proposed a scheme of building UPFC, which is a kind of equipment with a strong ability to control the power flow on the lines.

- *Scheme 4*: Build a 220 kV UPFC, of which the series sides are installed on the two lines from Longhai to Jiaozishan, and the parallel side of it is connected to a Jiaozishan 220 kV Bus, as shown in Figure 8. Based on the engineering experience, it is preliminarily determined that the capacity of the parallel end is 50 MVA, and the capacity range of each of the two series ends ranges from 50 MVA to 250 MVA. If built, the UPFC can directly control the power flow on the lines from Longhai to Jiaozishan, and then indirectly change the power flow on other problematic lines in Table 2.

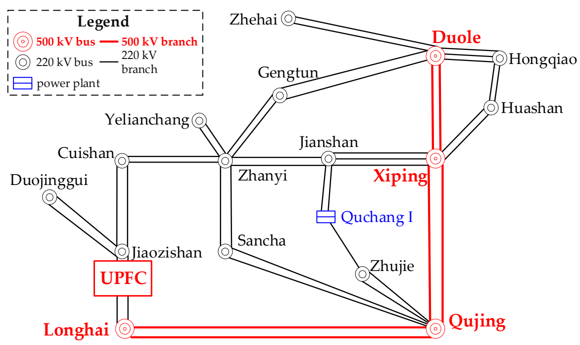

Figure 8. Sketch map of Scheme 4.

5.3. Calculation of the Weights of the Indicators

5.3.1. Subjective Weights

(a) The six evaluation indicators and the serial number of them are shown in Table 1.
(b) According to the analysis of the current situation of the Qujing Power Grid, the thermal stability margin is selected as the best indicator, and the proportion of the bus related to commutation failure is selected as the worst indicator.

(c) By comparison, the resulting best-to-others vector and the resulting other-to-worst vector can be obtained:

$$\boldsymbol{P}_{\mathrm{B}} = (5,\ 3,\ 2,\ 1,\ 3,\ 9) \tag{30}$$

$$\boldsymbol{P}_{\mathrm{W}} = (2,\ 3,\ 5,\ 9,\ 3,\ 1) \tag{31}$$

(d) Then, the subjective weights of the indicators can be calculated using (23).

5.3.2. Objective Weights

The normalized values of the six evaluation indicators used to calculate the objective weights are shown in Table 8. Then, the objective weights are calculated using (25).

Table 8. The normalized values of the six indicators used to calculate the objective weights.

Corresponding Scheme	r_{i1} ($K_{\mathrm{sc}i}$)	r_{i2} ($P_{\mathrm{Lmg}i}$)	r_{i3} (K_{time})	r_{i4} (ξ_i)	r_{i5} (μ)	r_{i6} ($K_{\mathrm{fail}j}$)
Scheme 1 (4 × JL/G1A-630/45)	0.3463	0.7277	0.6689	0.0722	0.6397	1.0000
Scheme 2 (4 × JL/G1A-630/45)	0.3654	0.7277	0.6528	0.0899	0.6397	1.0000
Scheme 3 (4 × JL/G1A-630/45)	0.3459	0.7285	0.6466	0.0336	0.6397	1.0000
Scheme 4 (50 MVA + 2 × 250 MVA)	0.4032	0.7563	0.6774	0.0433	0.6397	1.0000

5.3.3. Combined Weights

The combined weights are calculated using (27). The results are shown in Table 9.

Table 9. The weights of the six evaluation indicators.

Types of Weights	R_1 ($K_{\mathrm{sc}i}$)	R_2 ($P_{\mathrm{Lmg}i}$)	R_3 (K_{time})	R_4 (ξ_i)	R_5 (μ)	R_6 ($K_{\mathrm{fail}j}$)
Subjective weight (w_j')	0.08120	0.13675	0.20513	0.39743	0.13675	0.04274
Objective weight (w_j'')	0.16256	0.16181	0.16182	0.19031	0.16175	0.16175
Combined weight (w_j)	0.12059	0.15613	0.19123	0.28867	0.15611	0.08727

5.4. Comprehensive Evaluation of the Schemes

5.4.1. Evaluation of Scheme 1, Scheme 2, and Scheme 3

The estimated costs of Scheme 1, Scheme 2, and Scheme 3 are mainly related to the sectional area of the conductors. Meanwhile, based on the combined weights and the values of six indicators, the technical scores of the three schemes when selecting different conductors can be calculated. These results are all shown in Table 10. Accordingly, the technology-cost curves of these schemes are drawn, as shown in Figure 9.

Table 10. The estimated costs and the technical scores of Scheme 1, Scheme 2, and Scheme 3.

	Conductor Model	$F_1(i)$/RMB	$F_2(i)$/RMB	$F(i)$/RMB	Technical Score
Scheme 1	4 × JL/G1A-400/35	1.37×10^8	1.71×10^8	3.08×10^8	0.4842
	4 × JL/G1A-500/45	1.37×10^8	2.05×10^8	3.42×10^8	0.4898
	4 × JL/G1A-630/45	1.37×10^8	2.53×10^8	3.90×10^8	0.4913
Scheme 2	4 × JL/G1A-400/35	1.13×10^8	1.42×10^8	2.55×10^8	0.4887
	4 × JL/G1A-500/45	1.13×10^8	1.70×10^8	2.83×10^8	0.4945
	4 × JL/G1A-630/45	1.13×10^8	2.10×10^8	3.23×10^8	0.4956
Scheme 3	4 × JL/G1A-400/35	1.22×10^8	1.36×10^8	2.58×10^8	0.4673
	4 × JL/G1A-500/45	1.22×10^8	1.64×10^8	2.86×10^8	0.4742
	4 × JL/G1A-630/45	1.22×10^8	2.02×10^8	3.24×10^8	0.4759

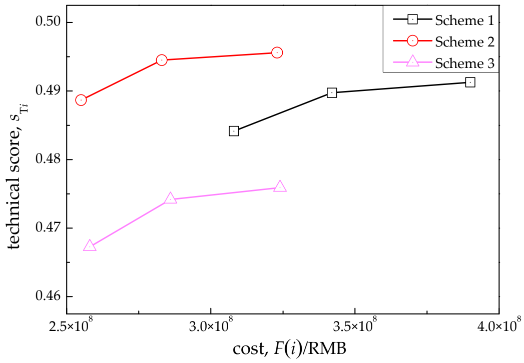

Figure 9. Technology-cost curves of Scheme 1, Scheme 2, and Scheme 3.

Due to the consideration of practice, only a limited number of conductor choices are considered in these three schemes. Therefore, only a limited number of points on each curve in Figure 9 correspond to the actual calculation results, while the whole dotted lines can only roughly fit the trends. Apparently, Scheme 2 is the best of the three schemes.

5.4.2. Comparison of Scheme 2 and Scheme 4

For Scheme 4, the estimated cost and the technical score are calculated repeatedly with the change of the series capacity of the UPFC, when the interval is 25 MVA. The results are shown in Table 11. After that, the technology-cost curve of Scheme 4 is drawn, as shown in Figure 10.

Table 11. The estimated costs and the technical scores of Scheme 4.

Parallel Capacity	Series Capacity	$F_1(i)$/RMB	$F_2(i)$/RMB	$F(i)$/RMB	Technical Score
50 MVA	2 × 50 MVA	1.33×10^8	5.40×10^7	1.87×10^8	0.4750
	2 × 75 MVA	1.33×10^8	8.10×10^7	2.14×10^8	0.4781
	2 × 100 MVA	1.33×10^8	1.08×10^8	2.41×10^8	0.4812
	2 × 125 MVA	1.33×10^8	1.35×10^8	2.68×10^8	0.4841
	2 × 150 MVA	1.33×10^8	1.62×10^8	2.95×10^8	0.4870
	2 × 175 MVA	1.33×10^8	1.89×10^8	3.22×10^8	0.4898
	2 × 200 MVA	1.33×10^8	2.16×10^8	3.49×10^8	0.4926
	2 × 225 MVA	1.33×10^8	2.43×10^8	3.76×10^8	0.4951
	2 × 250 MVA	1.33×10^8	2.70×10^8	4.03×10^8	0.4973

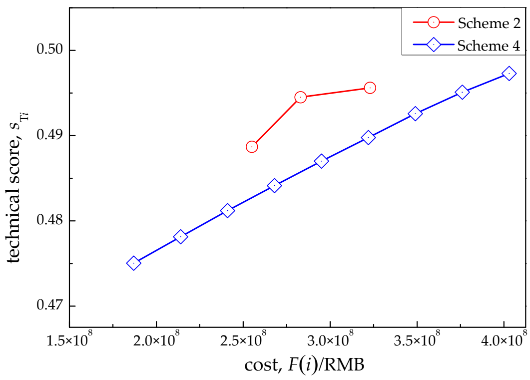

Figure 10. Technology-cost curves of Scheme 2 and Scheme 4.

According to Figure 10, it is obvious that the performance of Scheme 2 is better than that of Scheme 4. To sum up, for the strengthening of the Qujing Power Grid, Scheme 2 is the best of the schemes formulated in this paper. Moreover, considering the trend of the curve, the second type of conductor in Table 7 is recommended for Scheme 2, which will bring a total cost of RMB 283 million.

6. Conclusions and Future Scope

In this paper, an evaluation system is established to cover various safety and stability issues, and some typical countermeasures for the problems faced by AC/DC hybrid power grids are summarized. After that, a comprehensive evaluation method for AC/DC hybrid power grids and their strengthening schemes is proposed. By combining the multi-dimensional technical evaluation with the cost analysis, this method can give the technology-cost curves of different strengthening schemes. These curves reflect the relationships between the technical scores and the costs. Finally, the comprehensive evaluation method is implemented and verified in the case study of the Qujing Power Grid. The findings of this paper are drawn as follows.

- Once calculated, the technical score can reflect the stability and safety of a complex AC/DC hybrid power grid in an all-around way.
- Considering the technology-cost curves, the application values of different strengthening schemes can be easily judged for an AC/DC hybrid power grid.
- The main problem faced by the Qujing Power Grid is that the thermal stability margin of some lines may be insufficient in some single maintenance conditions. One of the schemes to build new AC lines is considered the best for this regional power grid.

Considering the increasing variety and quantity of power electronic equipment in China's State Grid, it is a feasible future research direction to put forward indicators which can reflect the influence of power electronic equipment more accurately. In addition, how to calculate and consider the cost in more detail is also content that can be studied later.

Author Contributions: Conceptualization, J.Z. and Z.X.; methodology, J.Z. and G.W.; software, J.Z.; validation, J.Z.; formal analysis, Z.X.; investigation, J.Z. and G.W.; resources, Z.Z.; data curation, J.Z.; writing—original draft preparation, J.Z.; writing—review and editing, G.W.; supervision, Z.Z. All authors have read and agreed to the published version of the manuscript.

Funding: This research received no external funding.

Data Availability Statement: Not applicable.

Conflicts of Interest: The authors declare no conflict of interest.

Abbreviations

The following abbreviations are used in this manuscript:

UPFC	unified power flow controller
HVDC	High-voltage direct current
VSC	voltage source converter
LCC	line commutated converter
HMESCR	hybrid multi-infeed effective short-circuit ratio
MTDC	multi-terminal direct current
RoCoF	rate of change of frequency
MCDM	multi-criteria decision making
AHP	analytic hierarchy process
BWM	best worst method
EWM	entropy weight method
TOPSIS	technique for order preference by similarity to ideal solution
MIIF	multi-infeed interaction factor
STATCOM	static synchronous compensator
FACTS	flexible AC transmission systems
RMB	Renminbi (Chinese currency)

Appendix A. Derivation of the Critical Clear Time of Fault

The detailed derivation of the critical clear time of the fault in Section 2.3 is given below.

In the derivation, values with subscript 0 are values before the fault, and values with superscript * are per-unit values.

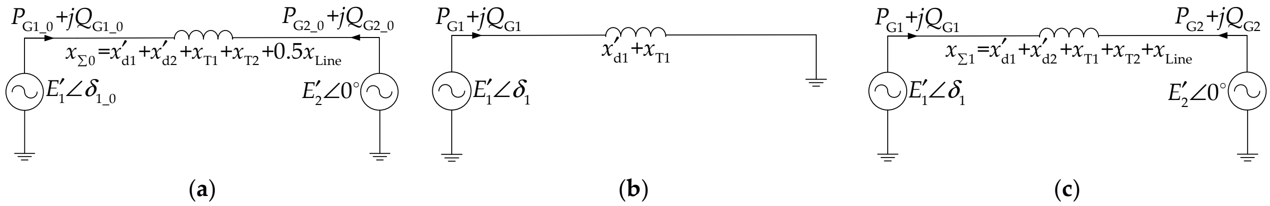

Figure A1. The circuit diagram of the two-area interconnected system. (**a**) Circuit before the fault occurs. (**b**) Circuit of Region 1 during the fault. (**c**) Circuit after the fault is clear.

The circuit diagram of the two-area system before the fault occurs is shown in Figure A1a. In this case, we have [29]:

$$P_{m1}{}^{*} - P_{D1}{}^{*} = P_{G1\_0}{}^{*} = \frac{E_1'{}^{*}E_2'{}^{*}\sin\delta_{1\_0}}{x'_{d1}{}^{*} + x'_{d2}{}^{*} + x_{T1}{}^{*} + x_{T2}{}^{*} + 0.5x_{Line}{}^{*}} \tag{A1}$$

Here, P_{m1} and P_{D1} are the mechanical power and damping power of G1, respectively.

We assume that the fault shown in Figure 3 occurs when $t = 0$. The circuit diagram of Region 1 during the fault is shown in Figure A1b. In this case, we have:

$$P_{G1}{}^{*} = 0 \tag{A2}$$

Then, according to the rotor motion equations, we have [29]:

$$\frac{T_{JG1}}{\omega_N}\cdot\frac{d^2\delta_1}{dt^2} = P_{m1}{}^{*} - P_{D1}{}^{*} - P_{G1}{}^{*} = P_{G1\_0}{}^{*} \tag{A3}$$

Here, δ_1 is the rotor angle of G1, and ω_N is the rated electric angular velocity of the rotor.

If the fault is cleared when $t = t_f$, and the rotor angle of G1 at that moment is set as δ_{1f}, then we have:

$$\delta_{1f} = \delta_{1\_0} + \frac{\omega_N P_{G1\_0}{}^{*}}{2T_{JG1}}t_f^2 \tag{A4}$$

The circuit diagram of the system after the clear of the fault is shown in Figure A1c. In this case, we have:

$$P_{G1}{}^{*} = \frac{E_1'{}^{*}E_2'{}^{*}\sin\delta_1}{x'_{d1}{}^{*} + x'_{d2}{}^{*} + x_{T1}{}^{*} + x_{T2}{}^{*} + x_{Line}{}^{*}} \tag{A5}$$

Then, the acceleration area (S1) and the deceleration area (S2) of G1 can be obtained, as shown in Figure A2a.

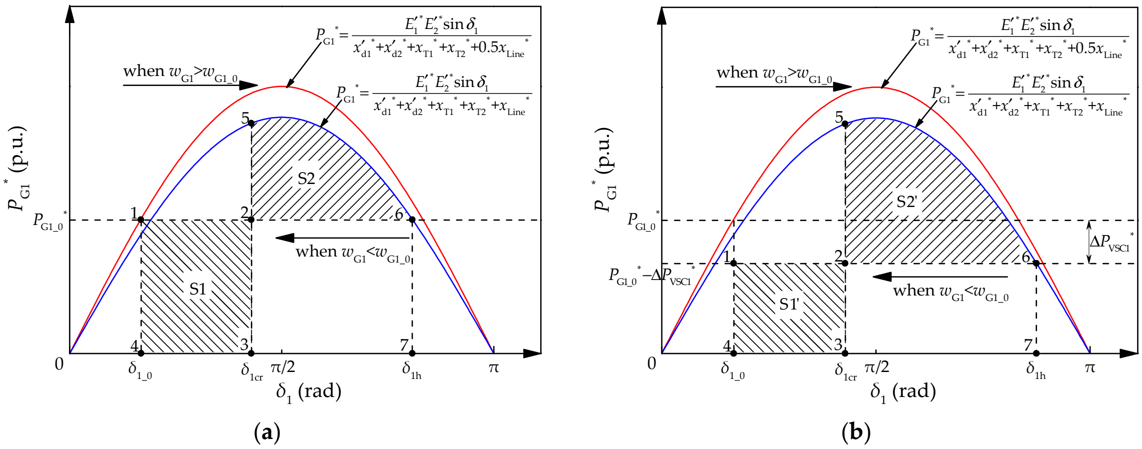

Figure A2. The acceleration area and the deceleration area. (**a**) Without the VSC-DC system. (**b**) With the VSC-DC system.

As described by the equal area criterion, in the critical case ($t_f = t_{cr}$, $\delta_{1f} = \delta_{1cr}$), the two areas should be equal, i.e:

$$\int_{\delta_{1\_0}}^{\delta_{1cr}} P_{G1\_0}{}^* d\delta_1 = \int_{\delta_{1cr}}^{\delta_{1h}} (P_{G1}{}^* - P_{G1\_0}{}^*) d\delta_1 \tag{A6}$$

As shown in Figure A2a, we have:

$$\frac{E_1'^* E_2'^* \sin\delta_{1\_0}}{x_{d1}'^* + x_{d2}'^* + x_{T1}{}^* + x_{T2}{}^* + 0.5x_{Line}{}^*} = \frac{E_1'^* E_2'^* \sin\delta_{1h}}{x_{d1}'^* + x_{d2}'^* + x_{T1}{}^* + x_{T2}{}^* + x_{Line}{}^*}, \quad \frac{\pi}{2} < \delta_{1h} < \pi \tag{A7}$$

Combining (A2)–(A7), we can get:

$$\begin{cases} t_{cr} = \sqrt{\dfrac{2T_{JG1}\cdot\left\{\cos^{-1}[\cos\delta_{1h} + (\delta_{1h} - \delta_{1\_0})\sin\delta_{1h}] - \delta_{1\_0}\right\}}{\omega_N P_{G1\_0}{}^*}} \\ \delta_{1h} = \pi - \sin^{-1}\left(\dfrac{x_{d1}'^* + x_{d2}'^* + x_{T1}{}^* + x_{T2}{}^* + x_{Line}{}^*}{x_{d1}'^* + x_{d2}'^* + x_{T1}{}^* + x_{T2}{}^* + 0.5x_{Line}{}^*}\sin\delta_{1\_0}\right) \end{cases} \tag{A8}$$

If the active power absorbed by VSC1 from the AC system is adjusted during and after the fault, (A3) can be modified as:

$$\frac{T_{JG1}}{\omega_N}\cdot\frac{d^2\delta_1}{dt^2} = P_{G1\_0}{}^* - \Delta P_{VSC1}{}^* \tag{A9}$$

Here, $\Delta P_{VSC1}{}^*$ is the increase in power absorbed by VSC1. This way, the acceleration area and deceleration area will change, as shown in Figure A2b. Thus, (A8) can be modified as:

$$\begin{cases} t_{cr} = \sqrt{\dfrac{2T_{JG1}\cdot\left\{\cos^{-1}[\cos\delta_{1h}\prime + (\delta_{1h}\prime - \delta_{1\_0})\sin\delta_{1h}\prime] - \delta_{1\_0}\right\}}{\omega_N(P_{G1\_0}{}^* - \Delta P_{VSC1}{}^*)}} \\ \delta_{1h}\prime = \pi - \sin^{-1}\left[\dfrac{(P_{G1\_0}{}^* - \Delta P_{VSC1}{}^*)x_{\Sigma 1}{}^*}{E_1'^* E_2'^*}\right] \\ x_{\Sigma 1}{}^* = x_{d1}'^* + x_{d2}'^* + x_{T1}{}^* + x_{T2}{}^* + x_{Line}{}^* \end{cases} \tag{A10}$$

References

1. State Council of the PRC. *The 14th Five Year Plan for National Economic and Social Development of the People's Republic of China and the Outline of Long-Term Objectives for 2035*; State Council of the PRC: Beijing, China, 2021. (In Chinese)
2. Li, M. Characteristic analysis and operational control of large-scale hybrid UHV AC/DC power grids. *Power Syst. Technol.* **2016**, *40*, 985–991. (In Chinese)

3. Liu, J.; Zhang, N.; Zhu, X.; Xu, K.; Chen, Z. Method of calculating the maximum transmission capability with unified power flow controller. *J. Eng.* **2017**, *13*, 1963–1968.
4. Xiao, H.; Sun, K.; Pan, J.; Li, Y.; Liu, Y. Review of hybrid HVDC systems combining line communicated converter and voltage source converter. *Int. J. Electr. Power Energy Syst.* **2021**, *129*, 106713. [CrossRef]
5. Dong, X.; Tang, Y.; Bu, G.; Shen, C.; Song, G.; Wang, Z. Confronting problem and challenge of large scale AC-DC hybrid power grid operation. *Proc. CSEE* **2019**, *39*, 3107–3119. (In Chinese)
6. Wang, F.; Liu, T.; Li, X. Decreasing the frequency of HVDC commutation failures caused by harmonics. *IET Power Electron.* **2017**, *10*, 215–221. [CrossRef]
7. Lü, P. Research on HVDC operation characteristics under the influence of hybrid AC/DC power grids. *Power Syst. Technol.* **2022**, *46*, 503–510. (In Chinese)
8. Ajaei, F.B.; Iravani, R. Dynamic interactions of the MMC-HVDC grid and its host AC system due to AC-side disturbances. *IEEE Trans. Power Deliv.* **2016**, *31*, 1289–1298. [CrossRef]
9. Dong, W.; Huang, M.; He, G.; Bao, W.; Wang, Y.; Liu, Q. An electromechanical-electromagnetic transient stability simulation system for AC/DC hybrid power system. *J. Syst. Simul.* **2021**, *33*, 2711–2719.
10. Ahrabi, R.R.; Li, Y.W.; Nejabatkhah, F. Unified control of the parallel LCC-VSCs interlinking converters in a hybrid AC/DC network. *IEEE Trans. Smart Grid* **2022**, *13*, 975–985. [CrossRef]
11. You, A.D.; Chen, B.Q.; Yin, C.X.; Wang, D.B. A study of electrical security risk assessment system based on electricity regulation. *Energy Policy* **2011**, *39*, 2062–2074.
12. Li, Y.; Wang, S.; Bu, G.; Yang, Y.; Zhao, B.; Wang, T. Analysis of the HVDC grid's influence on short-circuit current level of AC system. *J. Eng.* **2017**, *13*, 2098–2103. [CrossRef]
13. Nagao, T.; Tanaka, K.; Takenaka, K. Development of static and simulation programs for voltage stability studies of bulk power system. *IEEE Trans. Power Syst.* **1997**, *12*, 273–281. [CrossRef]
14. Kim, Y.K.; Lee, G.S.; Kim, C.K.; Moon, S.I. An improved AC system strength measure for evaluation of power stability and temporary overvoltage in hybrid multi-infeed HVDC systems. *IEEE Trans. Power Deliv.* **2022**, *37*, 638–649. [CrossRef]
15. Bu, S.; Du, W.; Wang, H. Probabilistic analysis of small-signal rotor angle/voltage stability of large-scale AC/DC power systems as affected by grid-connected offshore wind generation. *IEEE Trans. Power Syst.* **2013**, *28*, 3712–3719. [CrossRef]
16. Tang, C.; Graham, C.E.; El-Kady, M.; Alden, R.T.H. Transient stability index from conventional time domain simulation. *IEEE Trans. Power Syst.* **1994**, *9*, 1524–1530. [CrossRef]
17. Albu, M.; Dumitrescu, A.M.; Popovici, R. Rate of change of frequency—A power quality descriptor. In Proceedings of the IEEE 16th International Conference on Harmonics and Quality of Power (ICHQP), Bucharest, Romania, 25–28 May 2014.
18. Wang, B.; Sun, H.; Li, W.; Yan, J.; Yu, Z.; Yang, C. Minimum inertia estimation of power system considering dynamic frequency constraints. *Proc. CSEE* **2022**, *42*, 114–126. (In Chinese)
19. Shao, Y.; Tang, Y. Fast evaluation of commutation failure risk in multi-infeed HVDC systems. *IEEE Trans. Power Syst.* **2018**, *33*, 646–653. [CrossRef]
20. Saaty, T. A scaling method for priorities in hierarchical structures. *J. Math. Psychol.* **1977**, *15*, 234–281. [CrossRef]
21. Ishizaka, A.; Labib, A. Review of the main developments in the analytic hierarchy process. *Expert Syst. Appl.* **2011**, *38*, 14336–14345. [CrossRef]
22. Khan, M.Y.A.; ElKashouty, M.; Tian, F. Mapping groudwater potential zones using analytical hierarchical process and multicriteria evaluation in the Central Eastern Desert, Egypt. *Water* **2022**, *14*, 1041. [CrossRef]
23. Rezaei, J. Best worst multi criteria decision making method. *Omega* **2015**, *53*, 49–57. [CrossRef]
24. Rezaei, J. Best worst multi criteria decision making method—Some properties and a linear model. *Omega* **2016**, *64*, 126–130. [CrossRef]
25. Kumar, R.; Singh, S.; Bilga, P.S.; Jatin; Singh, J.; Singh, S.; Scutaru, M.L.; Pruncu, C.I. Revealing the benefits of entropy weights method for multi-objective optimization in machining operations: A critical review. *J. Mater. Res. Technol.* **2021**, *10*, 1471–1492. [CrossRef]
26. Luo, Y.; Li, Y. Comprehensive decision-making of transmission network planning based on entropy weight and grey relational analysis. *Power Syst. Technol.* **2013**, *37*, 77–81. (In Chinese)
27. Behzadian, M.; Otaghsara, S.K.; Yazdani, M.; Ignatius, J. A state-of-the-art survey of TOPSIS applications. *Expert Syst. Appl.* **2012**, *39*, 13051–13069. [CrossRef]
28. Diakoulaki, D.; Mavrotas, G.; Papayannakis, L. Determining objective weights in multiple criteria problems—The critic method. *Comput. Oper. Res.* **1995**, *22*, 763–770. [CrossRef]
29. Kundur, P. *Power System Stability and Control*; McGraw-Hill Professional: New York, NY, USA, 1994; pp. 184–187.
30. Zhu, X. *Fundamentals of Applied Information Theory*; Tsinghua University Press: Beijing, China, 2001; pp. 254–268. (In Chinese)